RSC Advances

PAPER

Check for updates

Cite this: *RSC Adv.*, 2020, **10**, 18360

Flotation separation of specularite from chlorite using propyl gallate as a collector

Xiangpeng Gao,[a] Fugang Zhao,[b] Mingyang Li*[ac] and Yiming Hu*[a]

Received 6th April 2020
Accepted 5th May 2020

DOI: 10.1039/d0ra03060k

rsc.li/rsc-advances

Separation of specularite from iron-containing silicate iron ore is challenging due to the similar surface properties of minerals and gangues. In this work, propyl gallate (PG) was applied as a chelating collector to separate specularite from chlorite. The flotation results indicated that collector sodium oleate (NaOL) shows little selectivity for the separation of specularite and chlorite. In contrast, the separation of specularite can be achieved with no depressant required when PG was used as the collector. The optimal separation results were obtained for single mineral flotation with recoveries of 87.11% and 6.98% for specularite and chlorite, respectively, and for mixed mineral flotation with 65.13% TFe grade and 76.28% TFe recovery, when the slurry pH was 8 and PG concentration was 40 mg L^{-1}. FT-IR and XPS analyses indicated that PG could be favorably adsorbed on specularite *via* phenolic hydroxyl groups, and molecular dynamic simulation results further elucidated the adsorption mechanism. This research suggested that the chelating flotation collector could be effective in the separation of minerals from iron-containing silicate iron ores.

1. Introduction

Iron ores, such as hematite, magnetite, specularite, *etc.*, are the basic materials of the iron and steel industries.[1,2] Due to the fast development of the economy and urbanization, the consumption of iron and steel requires more efficient separation methods to improve the grade of the ore.[3] Froth flotation has been proven to be one of the most effective processing methods for the separation of refractory iron ores.[4,5]

One of the refractory iron ores is iron-containing silicate type iron ore. It is difficult to separate in mineral processing due to the existence of the iron element in iron-containing silicates and iron ores, which leads to similar magnetic and floatability properties of targeted minerals and gangues.[6,7] It has been proven that the chlorite depressed by starch could not be floated effectively in reverse flotation route using anionic collector sodium oleate, and the addition of sodium alginate could improve the separation efficiency.[8] Besides, the sodium oleate also is invalid for the separation of hematite and aegirite; for example, the recovery of aegirite maintained around 80% while hematite around 90% with sodium oleate 1×10^{-4} mol L^{-1} at pH = 4–9.[9] Meanwhile, as for specularite and aegirite separation, these two minerals showed similar floatability when cationic collector dodecylamine was used.[7,10] Moreover, traditional depressants, including starch and carboxymethyl cellulose, were ineffective of selective depressing iron-containing silicates for the flotation separation of iron ores from amphibole or chlorite.[1,6,10,11] Hence, effective flotation reagents are urgently needed to solve the vexing beneficiation problems.

Chelating collectors can form metal chelates with minerals, which is more stable with metal than ionic and covalent bonds, has shown great potential in selective flotation.[11,12] As shown in Fig. 1, propyl gallate (PG), as known as propyl 3,4,5-trihydroxybenzoate, is an ester synthesized by condensation of gallic acid and propanol, which shows excellent solubility in a slurry. It appears as a fine white crystalline powder and widely used as an antioxidant to foods to prevent oxidation.[13] PG represents both hydrophobic and hydrophilic properties and has been applied as a chelating collector in the selective flotation of many minerals. PG can be used to collect scheelite and fluorite from calcite through oxygen atoms on the phenolic hydroxyl groups of PG binding to Ca atoms on the surface of the two minerals.[14,15] Benzene ring in a collector molecule usually contributes to the

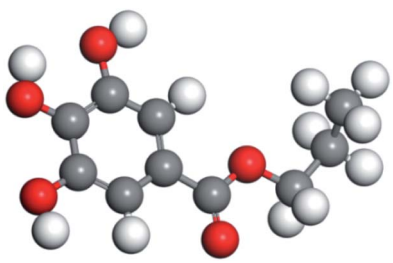

Fig. 1 Molecule structure of propyl gallate (PG) (the colour representation is as follows: white-hydrogen atoms; grey-carbon atoms; red-oxygen atoms).

[a]*Key Laboratory of Metallurgical Emission Reduction & Resources Recycling, Anhui University of Technology, Ministry of Education, Ma'anshan 243002, China. E-mail: my.l@ahut.edu.cn; yiminghu@ahut.edu.cn*

[b]*Sinosteel Maanshan Institute of Mining Research Co., Ltd., Ma'anshan 243071, China*

[c]*Faculty of Land and Resource Engineering, Kunming University of Science and Technology, Kunming 650093, China*

This article is licensed under a Creative Commons Attribution-NonCommercial 3.0 Unported Licence.

(cc) BY-NC

This journal is © The Royal Society of Chemistry 2020

frontier orbital. It is advantageous for donating electrons to the polar group, which enhances its reactivity and selectivity in flotation.[12] For example, PG was an effective collector separating diaspore from kaolinite, in which PG chelated with Al atoms on the diaspore surfaces by forming five-member rings through its *ortho* oxygens.[16]

Beside chelating with Ca and Al, PG shows excellent chelating property with Fe.[17] Due to that Fe concentration in specularite is much more than that of chlorite, which should make PG show more affinity to specularite and a potential collector for specularite/chlorite flotation. The use of PG to separate specularite from chlorite has not been reported. In this work, PG was applied as the chelating collector for specularite and chloride separation *via* forth flotation. The results indicated that PG showed excellent collecting property and selectivity for specularite through both hydrogen bonding interaction and chemical adsorption, while the collecting property for chlorite was quite faint. PG has excellent potentialities for iron-containing silicate type iron ore flotation.

2. Experimental

2.1 Materials

The pure chlorite and specularite samples were recieved from Yuanjiacun Mine (Shanxi Province, China) and Lilou Mine (Anhui Province, China), respectively. Both minerals were crushed before dry grinding by a porcelain ball mill. Then the grounded minerals were dry sieved into two size fractions samples (−74 + 37 μm and −37 μm).

For flotation and XRD analyses, the coarse size fraction sample (−74 + 37 μm) was used. The fine size fraction mineral sample (−37 μm) was thereafter grounded to −2 μm for FT-IR, zeta potential, and XPS analyses.

Analytical-grade propyl gallate (PG), sodium oleate (NaOL), starch, potassium chloride, sodium hydroxide, and hydrochloric acid were purchased from Adamas-beta® (Shanghai Titan Scientific Co.) and used as received.

2.2 Methods

2.2.1 Microflotation experiments. Microflotation experiments were carried out using a flotation machine (XFG-5) in a flotation cell (40 mL) with a mechanical agitation (1460 rpm). For single mineral flotation, 1 g specularite or chlorite sample and 30 mL deionized water was added into the flotation cell. The pH value of slurry was adjusted by 0.1 mol L^{-1} HCl or NaOH solution to designated value. The collector (NaOL or PG) was added and conditioned for 3 min, followed by 5 min flotation. Both concentrate and tailings were collected and completely dried in a drying oven at 80 °C to calculate the recovery. For mixed minerals flotation, 0.5 g specularite and 0.5 g chlorite were mixed in the flotation cell under the same flotation condition to single mineral flotation. All products were then dried, weighed, and assayed to calculate the recovery. All experiments were conducted for three times and average values were recorded.

2.2.2 X-ray patterns measurements. The X-ray diffraction (XRD) patterns of two minerals were characterized by using D8ADVANCE XRD equipment (Bruker, Germany) *via* the radiation (Cu Kα1) in the 2θ range of 5–90°.

2.2.3 Zeta potential tests. Zeta potential tests were determined by a ZetaPALS Zeta potential analyzer (Brookhaven Instruments Ltd. USA). In a typical set of measurement, 30 mg of specularite or chlorite sample (−2 μm) and 50 mL of 30 mg L^{-1} PG solution was added into a beaker with a magnetic stirrer (1500 rpm). 0.1 mol L^{-1} HCl or NaOH solution was used to adjust the pH value of the mixture. The zeta potential of samples was recorded after standing for 5 min in background electrolyte solution (KCl, 1.0×10^{-3} mol L^{-1}).

2.2.4 FT-IR measurements. FT-IR spectrums of specularite, PG, and specularite after PG adsorption were measured by a FT-IR spectrometer (Nicolet 6700, Thermo Fisher Scientific, USA) *via* KBr disc method. All measurements were tested at room temperature in the range of 400.0–4000.0 cm^{-1}. Specularite, PG, and specularite after PG adsorption were analyzed by mixing with potassium bromide powder and pressed into small pelletized discs before the measurements.

2.2.5 X-ray photoelectron spectroscopy. XPS measurements were conducted *via* an X-ray photoelectron spectrometer (Thermo ESCALAB 250XI, Thermo Fisher Scientific, USA) using monochromatic radiation (Al Kα) with 100 eV pass energy and 1 eV energy step size. The XPS measurements of specularite and specularite after PG adsorption were carried out by pressing the samples on a double side conductive adhesive carbon tape. High-resolution spectra of C 1s, O 1s, and Fe 2p were recorded and calibrated to the binding energy of C 1s at 284.8 eV.

2.2.6 Simulation method. Absorption of PG on chlorite and specularite were both calculated using the methods of molecular dynamics simulation (MDS). MDS was conducted using COMPASS force field and Forcite Plus module in Materials Studio (BIOVIA, San Diego, CA, USA).[18] The (001) surface was the most stable surface of chlorite and specularite, which was modelled for further adsorption calculation.[7,19] The bottom atoms fixed mineral face was geometry optimized using the smart algorithm method under 0.001 kcal mol^{-1} convergence accuracy. The Ewald summation procession was applied to calculate van der Waals force and electrostatic energy. The clave fractional depth of the (001) surface of chlorite and specularite was 3 and 2, respectively. Then these two surface models with 30 Å vacuum slab were extended to 4 × 4 and 5 × 8 unit cells, respectively. The initial velocity of the configuration was achieved by MDS with NVT ensemble. Then NVE ensemble was executed for essential MDS with 1 fs time step and 50 ps total simulation time. At last, MDS was calculated with NVT ensemble with 1 fs time step and 5000 ps total simulation time at 293 K.[20] The adsorption energy of PG on specularite and chlorite (001) surface was conducted in the DMol 3 module of Materials Studio software. The computational details were adopted as the available published paper.[21]

3. Results and discussion

3.1 XRD and elemental analysis

Fig. 2 illustrated the XRD patterns of specularite and chlorite samples. XRD peaks of specularite mainly correspond to the (012) and (024) Bragg's reflections of hexagonal structure of iron

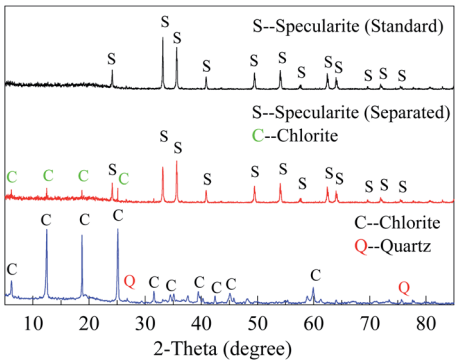

Fig. 2 X-ray diffraction patterns of specularite and chlorite samples.

Table 1 XRF analysis results of specularite and chlorite

	Content of each component/%						
Ore sample	Fe_2O_3	SiO_2	Al_2O_3	MgO	TiO_2	CaO	Na_2O
Specularite (standard)	95.74	3.36	0.38	0.23	—	—	—
Specularite (separated)	93.04	2.76	1.79	1.35	0.06	0.07	0.02
Chlorite	30.23	27.18	18.24	13.88	0.61	0.77	0.05

oxide while chlorite peaks are assigned to the monoclinic structure of $(Mg, Fe)_6(Si, Al)_4O_{10}(OH)_8$.[22] The X-ray fluorescence (XRF) results were shown in Table 1. The results indicated that both minerals have high purity, only with tiny amounts of quartz in the chlorite sample.

3.2 Microflotation tests

3.2.1 Microflotation of single minerals. Flotation separation of specularite and chlorite was firstly conducted by using NaOL as the collector. The results in Fig. 3(a) suggested that the recovery of both specularite and chlorite increases with increasing pH value from pH 2 to 10 and then decreased when the experimental pH value was over 10. The low floatability of the two minerals in acidic conditions are due to that NaOL is less ionized and the chemical adsorption of NaOL on specularite is not significant.[20] While the declined recoveries in alkaline conditions are caused by the increasing hydroxylation of metal species on the mineral surface, leading to the alternation of surface hydrophilicity; thus, the adsorption of NaOL on chlorite is significantly reduced in higher alkaline condition. Therefore, the optimum separation of two minerals can be found at pH 8, with an 89.82% recovery for specularite and a 73.91% recovery of chlorite. The desirable NaOL concentration for the separation of specularite and chlorite was studied at pH value 8 with NaOL concentration from 0 to 60 mg L^{-1}. It is as expected that the recoveries of two minerals both increased with increasing collector concentration, and kept steady after the NaOL concentration higher than 45 mg L^{-1}, in which the recovery of specularite and chlorite was 90.57% and 53.87%, respectively. Therefore, the optimum NaOL dosage was selected as 45 mg L^{-1}.

The separation of specularite and chlorite by collector NaOL is not very effective. Hence, an efficient collector for specularite and

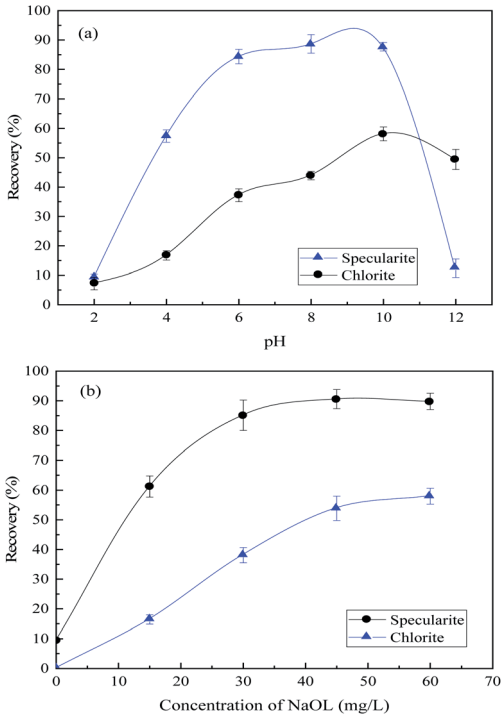

Fig. 3 Recovery of specularite and chlorite by NaOL as the collector (a) as a function of pH values with NaOL concentration of 45 mg L^{-1}; (b) as a function of NaOL dosage at pH 8.

chlorite separation in the neutral condition is urgently needed. Fig. 4(a) shows the floatability of two minerals as a function of pH values with 30 mg L^{-1} of PG. The recovery of chlorite remains lower than 15% under all pH conditions, while the floatability of specularite maintained high position, and the optimum recovery of specularite (90.17%) can be observed in faintly acid and neutral conditions (pH 4–8). By careful consideration, the slurry pH value was better determined as 8. Moreover, the effect of PG concentration was examined at pH 8 and results in Fig. 4(b) revealed that the floatability of specularite increased sharply with increasing of PG concentration from 10 mg L^{-1} to 40 mg L^{-1}, and specularite can be quantitatively recovered at 90.17% with PG dosage of 40 mg L^{-1}. While the recovery of chlorite remained low (less than 10%) under experimental conditions, which consisted with the results in Fig. 4(a).

3.2.2 Microflotation of mixed minerals. Flotation experiments of mixed minerals were conducted to evaluate the effect of PG on the separation of specularite and chlorite. As illustrated in Fig. 5(a), the total iron (TFe) grade of concentrate decreased slightly at first and then dropped sharply in the pH range of 4–12; in the meantime, the TFe recovery increased firstly then decreased with increasing slurry pH and the optimal TFe recovery 76.87% was reached at pH 8. It indicated that the relatively high separation results could be achieved under pH range 8–10.

Fig. 5(b) demonstrated that the TFe grade of concentrate decreased from 65.52% to 62.17% slightly, and the TFe recovery increased from 27.44% to 76.20% as the PG concentration increased. In summary, the optimum flotation can be achieved with a 65.13% TFe grade and 76.28% TFe recovery in concentrate,

 This journal is © The Royal Society of Chemistry 2020

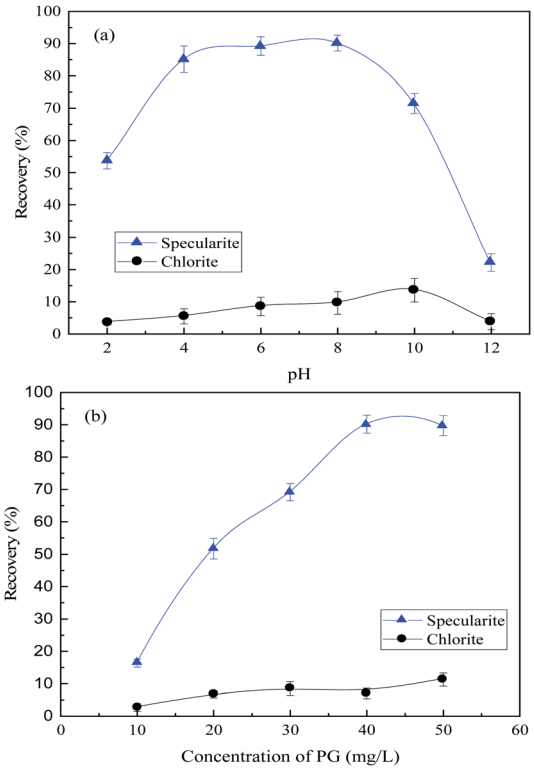

Fig. 4 Recovery of specularite and chlorite by PG as the collector (a) as a function of pH values with PG concentration of 40 mg L^{-1}; (b) as a function of PG dosage at pH 8.

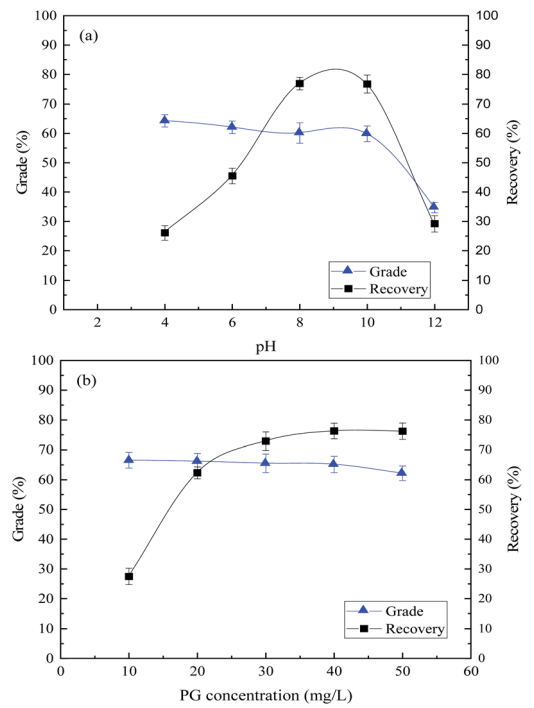

Fig. 5 Flotation of mixed minerals. (a) Effect of slurry pH with 40 mg L^{-1} PG; (b) effect of PG concentration at pH 8.

Table 2 Results of flotation concentrate with different collectors

Reagents	Concentration (mg L^{-1})	TFe grade (%)	TFe recovery (%)
NaOL[23]	60	51.91	62.78
CY-23 (ref. 23)	100	59.78	74.55
PG	40	65.13	76.28

when the corresponding slurry pH was 8 and PG concentration of 40 mg L^{-1}. The XRF analysis results of the concentrate are shown in Table 1, in which minor of chlorite mixed in the concentrate. The flotation results demonstrated that PG could separate specularite from chlorite effectively as a collector. The optimum flotation separation results with NaOL, CY-23 and PG as the collector, respectively, are shown in Table 2. Table 2 reveals that, compared with NaOL and CY-23, PG shows the best separation properties with higher TFe grade and recovery and lower consumption, which indicates PG is an excellent collector for specularite/chlorite separation.

3.3 Zeta potential measurements

Zeta potential of specularite and chlorite were recorded with and without PG adsorption (40 mg L^{-1}) to investigate the interactions between PG and the minerals. As indicated in Fig. 6, the results suggested that zeta potential values of these two minerals are highly depended on the pH values in which the surface charge of two minerals decreases with increasing pH value. Fig. 6(a) depicted that the iso-electric point (IEP) of specularite was 5.06, which was coincident with previous studies.[7,23] After PG was adsorbed on specularite, the zeta potential value shifted towards

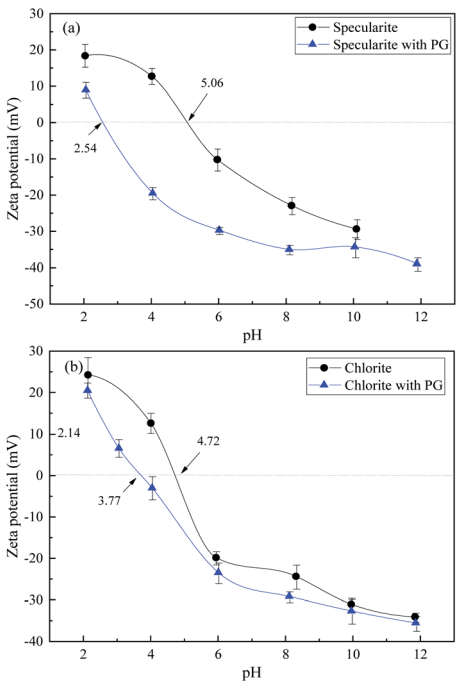

Fig. 6 Zeta potentials of specularite (a) and chlorite (b) as a function of pH in the absence and presence of 30 mg L^{-1} of PG.

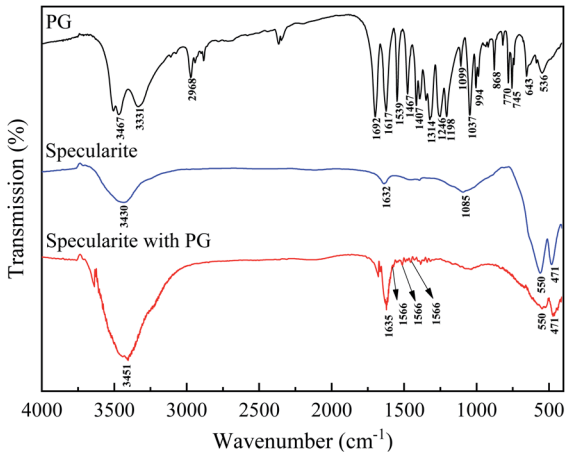

Fig. 7 FT-IR spectra of PG, specularite, and specularite after PG adsorption.

the negative direction significantly, and its extent enlarged in the pH range of 4–8. The IEP of specularite after PG adsorption shifted left to 2.54, which revealed that PG could adsorb onto the specularite surface strongly.

As shown in Fig. 6(b), the IEP of chlorite was 4.72, which was consistent with previous studies.[24] The zeta potential of chlorite after PG adsorption coincided with raw chlorite, illustrating that only a feeble reaction occurred between chlorite surfaces and PG molecule. In comparison, the involvement of PG brought the zeta potential of specularite more negative than chlorite, supporting that more amount of PG was adsorbed onto specularite than chlorite.

The specularite surface was negatively charged when the pH value is higher than 5.06, which was due to adsorption of hydroxyl on the mineral surface generated from comminution. When the pH value increased to around 8, ions were the main existing form of PG due to the protonation of hydroxyl groups.[15,17] In this case, electrostatic forces should not exist between specularite surfaces and PG. Thus the high recovery of specularite was mainly due to the chemical or hydrogen bond adsorption between PG and specularite.

3.4 FT-IR spectra analysis

FT-IR spectra of PG, specularite, and specularite after PG adsorption were recorded in Fig. 7.

Characteristic peaks for PG include: O–H stretching vibration at 3467 and 3331 cm^{-1};[13,16,25] C–H stretching vibrations of benzene ring at 2968 cm^{-1};[14] 1692 cm^{-1} is assigned to C=O stretching of ester; several consistent peaks at 1617, 1539 and 1467 cm^{-1} due to C=C stretching in phenyl group and phenolic C–H bending vibration, respectively;[26,27] 1314 cm^{-1} attributed to phenol O–H bending; 1246, 1198, and 1099 cm^{-1} caused by C–O–C stretching from aromatic ester;[28] 994, 868, 770, and 745 cm^{-1} attributed to C=C bending and angular deflections of the C–H fragment, respectively.[26] For specularite, peaks at 3430 and 1632 cm^{-1} are attributed to absorbed water. Peaks at 550 and 471 cm^{-1} are due to the formation of hematite.[29] After PG adsorption, the –OH stretching vibration bands (3520–3330 cm^{-1}) of PG becomes unobvious in specularite after PG adsorption, demonstrating that the –OH group deprotonated and formed the O–Fe bonds. The C=O stretching vibration peak (1670 cm^{-1}) and C–O–C stretching peaks (1250–1000 cm^{-1}) indicated the interaction of between the ester group and Fe atoms in specularite did not occur. The C=C stretching peaks in phenyl group shifted from 1617, 1539 and 1467 cm^{-1} to 1566, 1503 and 1444 cm^{-1}, which was mainly caused

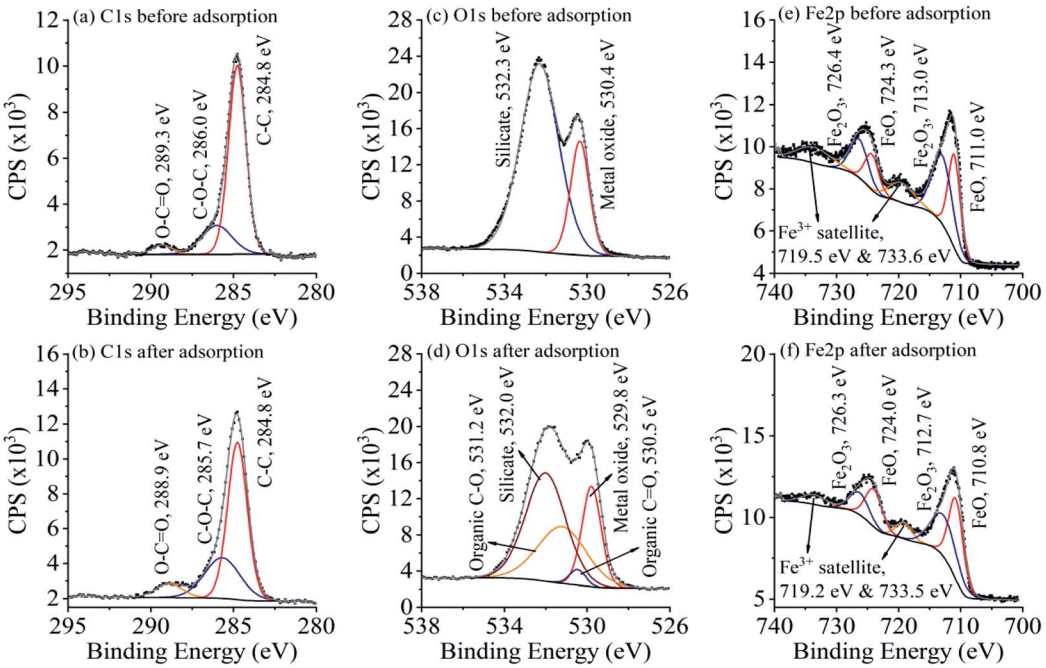

Fig. 8 XPS spectra of C 1s (a and b), O 1s (c and d), and Fe 2p (e and f) before and after PG adsorption with their deconvoluted fitting curves.

 This journal is © The Royal Society of Chemistry 2020

by transfers of the conjugative π electrons through after the chelation between deprotonated hydroxyl of PG with Fe atoms.[17]

3.5 XPS analysis

In order to affirm the adsorption mechanism, XPS analyses were conducted for specularite before and after PG adsorption to evaluate the electron migration in the adsorption process. High-resolution spectra of C 1s, O 1s, and Fe 2p with their deconvoluted fitting curves were illustrated in Fig. 8. C–C peak at 284.8 eV was used to calibrate the binding energy scale for all measurements. Two other peaks in C 1s (Fig. 8(a)) correspond to carbon contamination, and their intensity increased after PG adsorption in Fig. 8(b), which refers to the ester and carboxyl groups on PG molecules.[30] O 1s exists in two forms on specularite sample, 530.4 and 532.3 eV for metal oxide and silicate, respectively.[31–33] After PG adsorption, two peaks both shifted to lower binding energies, indicating that oxygen atoms act as electron acceptors during the adsorption process. Two new peaks at 530.5 and 531.2 eV can be observed in Fig. 8(d), which are assigned to C=O and C–O, respectively. Fe 2p region contain split spin–orbit components of Fe $2p_{1/2}$ and Fe $2p_{3/2}$ with a 13.3 eV difference of binding energy.[34–36] Deconvoluted peaks in Fig. 8(e) correspond to FeO, Fe_2O_3, and Fe^{3+} satellite, which all shifted to lower binding energies due to the acceptance of electrons from PG. XPS results concluded that oxygen and iron atoms were the electron acceptors in the adsorption of PG, which was consisted with the FT-IR results.

3.6 Molecular dynamics simulation

The equilibrium snapshots of PG on the (001) surface of specularite and chlorite was further studied by MDS. Fig. 9 showed the equilibrium configuration of PG on each mineral. The results from Fig. 9(a) indicated that the adsorption of PG on specularite mainly occurred by the chelate bond between O atoms in polar components of PG and Fe atoms on specularite (red line) and hydrogen bond between H atoms in PG and O atoms on specularite (blue line). As observed in Fig. 9(b), PG adsorbed on chlorite surface mainly due to the hydrogen bond between H atoms in PG and O atoms on chlorite. By contrast, PG was closer to the specularite surface than chlorite. Moreover, PG was aggregated on the specularite surface and formed a compact configuration compared to the adsorption on chlorite. The results suggested that PG was more favourably adsorbed on specularite, which was consistent with FT-IR and XPS analyses.

Fig. 10 presented the relative concentration of PG along the *z*-direction, which was normal to the (001) surface of specularite and chlorite. The distribution of PG on specularite and chlorite surface was quantified through the relative concentration calculation of atoms O in the de-protonated hydroxyl in the *para*-position and H atoms in benzene ring and hydrocarbon chain of PG. The nearest atoms to the surface should be the primary action point.[20] After PG acted with specularite, atoms O distributed at a distance of 1–15 Å with the strongest one being at 2.85 Å than that of H atoms 2.93 Å. The results indicated that PG adsorbed on the specularite surface *via* atoms O acting with surface Fe. While as for chlorite, the most reliable bond distance of O and H atoms was 3.34 Å and 3.19 Å, respectively, which means that PG ions adsorbed on chlorite surface mainly with H atoms. By comparing these two models with the same kind of atoms, the distance of most atoms O and H in PG on the specularite surface was smaller than that of chlorite. In other words, PG had stronger interaction with specularite than chlorite.

Adsorption energy of PG on specularite and chlorite (001) surface was further calculated to compare PG's affinity to these two minerals. The results revealed that the adsorption energy of PG on specularite and chlorite was −1.03 eV and −0.24 eV, respectively, which indicates that the affinity of PG to specularite is much more than to chlorite. The affinity of PG to the

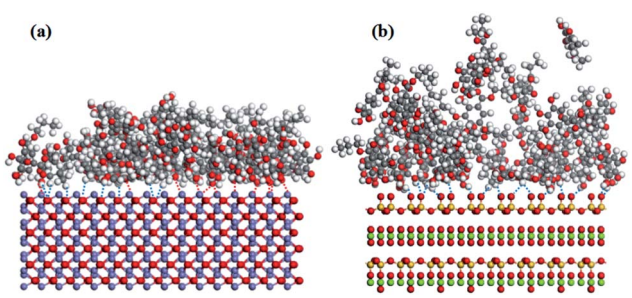

Fig. 9 Adsorption configuration of PG on the surface of (a) specularite; (b) chlorite (the colour representation is as follows: white-hydrogen atoms; grey-carbon atoms; red-oxygen atoms; purple: iron atoms; yellow-silicon atoms; green-metal ions in chlorite).

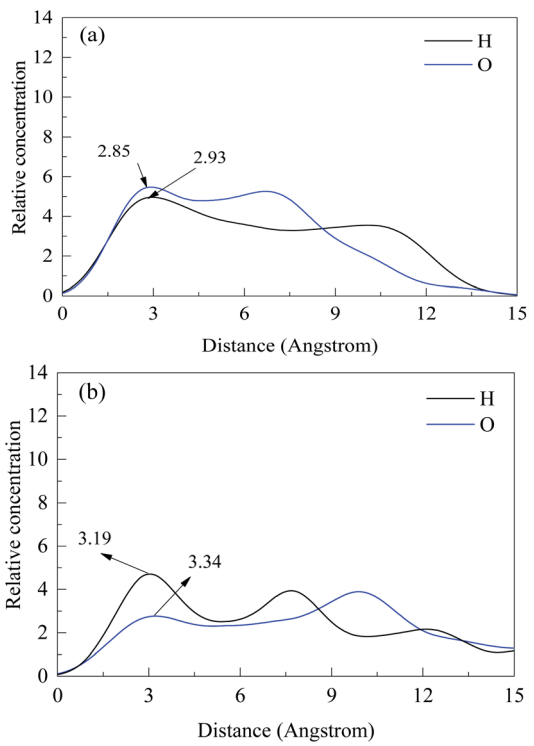

Fig. 10 *z*-Direction relative concentration profiles of hydrogen and oxygen in PG on (a) specularite and (b) chlorite.

two minerals is concordant with the experiments, detection, and MD simulation results above.

As a phyllosilicate mineral, chlorite is comprised of the silicon–oxy tetrahedron and metallic oxide with the ratio of 2 : 1. The content Fe of chlorite is less than specularite, and the high solubility of metallic oxide on chlorite surface in slurry makes further efforts of the decreasing content of surface Fe. Due to that, PG adsorbs onto minerals mainly *via* chemical adsorption between O atoms in the de-protonated hydroxyl and Fe atoms on the mineral surface. Therefore, the difference in surface Fe content causes the selectivity difference for specularite and chlorite. Based on these ratiocinations, PG also should be a valid collector for separating specularite or hematite from iron-containing silicates, such as aegirite, grunerite, ferrodolomite, *etc.*, especially for separating iron oxide from gangue quartz.

4. Conclusions

Specularite and chlorite were separated by flotation using PG as a facile collector. The results indicated that the optimum separation could be achieved for single mineral flotation with recovery 87.11% for specularite and 6.98% for chlorite, and for mixed minerals, the optimum results were obtained with 65.13% TFe grade and 76.28% TFe recovery respectively at pH 8 and PG concentration 40 mg L^{-1}, which is superior to NaOL as a conventional collector. Zeta potential, FT-IR, and XPS analyses have demonstrated that PG can be favorably adsorbed on specularite than chlorite by interactions with oxygen and iron atoms, resulting in the recoveries difference of two minerals. Molecular dynamics calculation further elucidated the binding configurations of PG on specularite and chlorite, which is highly consistent with characterization results. In conclusion, PG could be an efficient collector to float iron ore from iron-containing silicates.

Conflicts of interest

There are no conflicts to declare.

Acknowledgements

We gratefully appreciate the financial support from the National Natural Science Foundation of China (grant numbers 51904001, 51674001), the Key Research and Development Projects of Anhui Province (grant numbers 201904a07020054, 201904a07020044); and Key Laboratory of Metallurgical Emission Reduction & Resources Recycling (grant number JFK19-01 and JFK20-05).

Notes and references

1 L. O. Filippov, V. V. Severov and I. V. Filippova, *Int. J. Miner. Process.*, 2014, **127**, 62–69.
2 W. Liu, W. Liu, Q. Zhao, Y. Shen, X. Wang, B. Wang and X. Peng, *J. Mol. Liq.*, 2020, **301**, 112428.
3 X. Zhang, X. Gu, Y. Han, N. Parra-Álvarez, V. Claremboux and S. K. Kawatra, *Miner. Process. Extr. Metall. Rev.*, 2019, 1–29.
4 L. O. Filippov, I. V. Filippova and V. V. Severov, *Miner. Eng.*, 2010, **23**, 91–98.
5 A. C. Araujo, P. R. M. Viana and A. E. C. Peres, *Miner. Eng.*, 2005, **18**, 219–224.
6 L. O. Filippov, V. V. Severov and I. V. Filippova, *Int. J. Miner. Process.*, 2013, **123**, 120–128.
7 M. Li, J. Liu, X. Gao, Y. Hu, X. Tong, F. Zhao and Q. Yuan, *Minerals*, 2019, **9**, 782.
8 Y. Fu, W. Yin, B. Yang, C. Li, Z. Zhu and D. Li, *Int. J. Miner., Metall. Mater.*, 2018, **25**, 1113–1122.
9 G. Mei, X. Mai and Y. Yu, *Met. Mine.*, 2002, 18–20.
10 M. Li, J. Liu, Y. Hu, X. Gao, Q. Yuan and F. Zhao, *Carbohydr. Polym.*, 2020, **240**, 116334.
11 X. Yang, S. Liu, G. Liu and H. Zhong, *J. Ind. Eng. Chem.*, 2017, **46**, 404–415.
12 Y. Li, Y. Liu, J. Chen and C. Zhao, *Miner. Eng.*, 2020, **146**, 106133.
13 A. D. Wilson and D. T. Lewis, *Analyst*, 1963, **88**, 585–589.
14 J. Gao, W. Sun, Y. Hu, L. Wang, R. Liu, Z. Gao, P. Chen, H. Tang, W. Jiang and F. Lyu, *Chem. Eng. Sci.*, 2019, **193**, 255–263.
15 F. Lyu, J. Gao, N. Sun, R. Liu, X. Sun, X. Cao, L. Wang and W. Sun, *Miner. Eng.*, 2019, **131**, 66–72.
16 F. Lyu, W. Sun, S. A. Khoso, C. Zhang, R. Liu, L. Wang and J. Gao, *Miner. Eng.*, 2019, **133**, 19–26.
17 N. Binbuga, K. Chambers, W. P. Henry and T. P. Schultz, *Holzforschung*, 2005, **59**, 205–209.
18 A. Klamt and G. Schüürmann, *J. Chem. Soc., Perkin Trans. 1*, 1993, **2**, 799–805.
19 E. J. Silvester, W. J. Bruckard and J. T. Woodcock, *Miner. Process. Extr. Metall.*, 2011, **120**, 65–70.
20 L. Li, H. Hao, Z. Yuan and J. Liu, *Appl. Surf. Sci.*, 2017, **419**, 557–563.
21 S. S. Rath, H. Sahoo, B. Das and B. K. Mishra, *Miner. Eng.*, 2014, **69**, 57–64.
22 C. H. Veloso, L. O. Filippov, I. V. Filippova, S. Ouvrard and A. C. Araujo, *Miner. Eng.*, 2018, **125**, 133–139.
23 W. Liu, X. Peng, W. Liu, X. Wang, Q. Zhao and B. Wang, *Powder Technol.*, 2020, **360**, 1117–1125.
24 T. Yue and X. Wu, *Minerals*, 2018, **8**, 85.
25 W. Jiang, Y. Zhou and Y. Zhang, *Chem*, 2018, **2018**, 1–6.
26 D. Fornasiero and J. Ralston, *Int. J. Miner. Process.*, 2005, **76**, 75–81.
27 U. L. Kala, S. Suma, M. R. P. Kurup, S. Krishnan and R. P. John, *Polyhedron*, 2007, **26**, 1427–1435.
28 W. Wang, Q. Chen, C. Jiang, D. Yang, X. Liu and S. Xu, *Colloids Surf., A*, 2007, **301**, 73–79.
29 M. I. F. Barbosa, R. S. Corrêa, K. M. de Oliveira, C. Rodrigues, J. Ellena, O. R. Nascimento, V. P. C. Rocha, F. R. Nonato, T. S. Macedo, J. M. Barbosa-Filho, M. B. P. Soares and A. A. Batista, *J. Inorg. Biochem.*, 2014, **136**, 33–39.
30 M. Massoni, J. C. T. Clavijo, L. Colina-Vegas, W. Villarreal, J. S. M. Dias, G. A. F. da Silva, M. Ionta, M. Soares, J. Ellena, A. C. Dorigueto, M. I. F. Barbosa and A. A. Batista, *Polyhedron*, 2017, **129**, 214–221.

 This journal is © The Royal Society of Chemistry 2020

31 Y. Wang, A. Muramatsu and T. Sugimoto, *Colloids Surf., A*, 1998, **134**, 281–297.
32 M. C. Burrell, Y. S. Liu and H. S. Cole, *J. Vac. Sci. Technol., A*, 1986, **4**, 2459–2462.
33 X. Gao, J. Liu, M. Li, C. Guo, H. Long, Y. Zhang and L. Xin, *Chem. Eng. J.*, 2020, **385**, 123897.
34 J. Liu, M. Ejtemaei, A. V. Nguyen, S. Wen and Y. Zeng, *Miner. Eng.*, 2020, **145**, 106058.
35 M. Mullet, V. Khare and C. Ruby, *Surf. Interface Anal.*, 2008, **40**, 323–328.
36 T. Yamashita and P. Hayes, *Appl. Surf. Sci.*, 2008, **254**, 2441–2449.